| JMATPRO | Journal of Advanced Materials and Processing<br>10 (1): 13-26, Winter 2022<br>http://jmatpro.iaun.ac.ir<br>20.1001.1.2322388.2022.10.1.2.5 |
|---|---|

Research Paper

# Development and Evaluation of Nanomagnetic Carrier for the Controlled Loading and Release of Celecoxib

**Shabnam Ahmadvand [1], Maryam Kargar Razi[1*], Babak Sadeghi [2], Seyedeh Sara Mirfazli [3]**

*1. Department of Chemistry, Islamic Azad University, North Tehran Branch, Tehran, Iran*
*2. Department of Chemistry, Islamic Azad University, Tonekabon Branch, Tonekabon, Iran*
*3. Department of Medicinal Chemistry, School of Pharmacy International Campus, Iran University of Medical Sciences, Tehran, Iran*

**ARTICLE INFO**

*Article history:*

Received 22 October 2021
Accepted 19 December 2021
Available online 1 January 2022

*Keywords:*
*Dynamic Light Scattering (DLS)*
*Magnetite*
*Nanocomposite*
*Celecoxib*
*TGA*

**ABSTRACT**

The aim of the present study was to develop synthesize, characterize, and find many applications of functionalized metal oxide nanoparticles. Herein, a new strategy is developed to functionalize magnetite nanoparticles to improve their performances of cerium oxide-functionalized $Fe_3O_4$@$SiO_2$@$CeO_2$ magnetic nanoparticles (FSC). In this study, after preparing optimized FSC, characterization and identification of their chemical structure were carried out by FT-IR, FESEM, VSM, TGA, DLS, and XRD. Afterward, the functionalized nanoparticles were examined in the delivery of celecoxib as an active drug model involving cerium oxide and hydroxyl functional groups. The results with respect to particle size, present investigation indicate that the formulations ($m_{FSC}$=5 mg, pH=3.3) can be considered as best among various formulations. Dynamic light scattering (DLS) techniques used to measure particle size and zeta potential distribution revealed successful preparation of an $Fe_3O_4$@$SiO_2$@$CeO_2$ nanocomposite prepared on $Fe_3O_4$@$SiO_2$ (FS), with a hydrodynamic size distribution of 45 nm.

**Citation**: Ahmadvand, Sh.; Kargar Razi, M.; Sadeghi, B.; Mirfazli, S.S. (2022) Development and Evaluation of Nanomagnetic Carrier for the Controlled Loading and Release of Celecoxib, Journal of Advanced Materials and Processing, 10 (1), 13-26. Dor: 20.1001.1.2322388.2022.10.1.2.5



* **Corresponding Author.**
E-mail Address: m_kargarrazi@iau-tnb.ac.ir

## 1. Introduction

In regeneration, nanomaterials with biomaterials are offer ways to control surface and mechanical properties. Moreover, it increases cellular adhesion, differentiation, and integration of stem cells into the environment around us. Finally, the additional possibilities of increasing the biological performance of biomaterials are because of the drug delivery capabilities of nanoparticles [1].

The use of nanotechnology to improve current approaches in tissue and organ regeneration has received increased attention over the years owing to the great versatility that they offer in terms of size and surface chemistry, allowing the utilization as carriers for the delivery of drugs, genetic material, or growth factors (GFs). Indeed, various nanoparticles have been developed for therapy; these include dendrimers, liposomes, polymer-based nanoparticles, micelles, carbon nanotubes, and many more [2]. The slower transit times exhibit regarding nanoparticulate oral delivery systems than larger-sized particles in various dosage forms, increasing the local concentration gradient across absorptive cells, thereby enhancing local and systemic delivery of both free and bound drugs across the gut [3].

A number of biocompatible carrier systems involving large surface areas and tailorable pore size are introduced for drug delivery, such as calcium phosphate cement [4], organic polymers [5], various inorganic composites [6], metal-organic frameworks [7], and nanoporous silica [8, 9].

In regeneration, nanoparticles improve biomaterials' regenerative capabilities, offering ways to control surface and mechanical properties. Moreover, the incorporation of nanoparticles within biomaterials increases cellular adhesion, differentiation, and integration of stem cells into the surrounding environment [10]. Inevitably, the release rate of drugs can be affected by important parameters such as pores size and functional groups anchored to the surface of the carrier [11]. The modification in the surface and properties could be effective [12] and make the pores interact with drugs and control drug delivery processes [13]. Magnetic iron oxide nanoparticles with a large surface area, due to their multifunctional properties, superparamagnetism, and low toxicity, have been known as potential carriers in drug delivery for applications in medicine and biology [14-16]. The purpose of this investigation is to construct developed a new strategy to functionalize $Fe_3O_4$ by $CeO_2$ and well-ordered magnetic core/mesoporous shell $Fe_3O_4@SiO_2$ spheres. Then, the fabricated nanocarrier was used for the promising delivery of celecoxib as a model antiviral drug [17-20]. Influences of the type and concentration of the surfactant, pH, contact time, and temperature on the loading/release of celecoxib, loading capacity, and in vitro potential for drug adsorption enhancement of $Fe_3O_4@SiO_2@CeO_2$ magnetic nanoparticles (FSC) are systematically investigated.

## 2. Experimental

### 2.1. Methods and Materials

All chemicals were received from commercial resources (Merck and Chem Lab) and utilized without further refinement. Field emission scanning electron microscope (FESEM) micrographs were taken by applying an LEO 440i (acceleration speed voltage 26 kV). FT-IR spectra were recorded on a Bomem MB100. These measurements were carried out at a resolution of 4 $cm^{-1}$ in KBr pellets. The pellets have been used for FTIR spectroscopy measurement.

The particle size of HA/casein nanoparticles was measured using Dynamic Light Scattering (DLS) technique (ZS/ZEN3600 Zeta sizer; Malvern, Instruments Ltd, Malvern, UK). The crystalline structure of the samples was assessed by X-ray diffraction (XRD) analysis on a Seisert Argon 3003 PTC using nickel filtered XD-3Cu Ka radiations (k = 1.5418 A). A freeze dryer, Model FD-10, Pishtaz Equipment Engineering Co, Iran, was applied for drying of the prepared nanomaterials. $Fe_3O_4$ and $Fe_3O_4@SiO_2@CeO_2$ nanocomposites were synthesized by the introduced single-step solvothermal method with a few modifications [20-22].

### 2.2. Preparation

$Fe_3O_4$ nanoparticles were prepared similar to the method reported in several studies [20-22]. $FeCl_3.6H_2O$ (2.2 g), $NaNO_3.3H_2O$ (0.42 g), PEG-400 (53 ml), and 6 ml ethanol were mixed under intense stirring at 25 °C for 40 min. Then, 3 g of NaAc was added, and the resulting was mixed under intense stirring at 25 °C for 14 h. After that, the mixture was put on a stainless steel autoclave (with Teflon-lined) of 60 ml volume. Eventually, the autoclave was warmed and retained at 190 °C for 12 h, and afterward, it was chilled off to room temperature. The particles were washed three times with absolute ethanol and were dried by a rotary evaporator [18].

A one-step synthesis was used to obtain silica-coated $Fe_3O_4$ nanoparticles. 0.15 g of $Fe_3O_4$ was dispersed in a mixture containing distilled water (3 ml), absolute ethanol (7 ml), and ammonia (0.3 ml, 25%) with sonication for 40 min. Then, the reaction mixture was conducted with 0.7 ml *cetyltrimethylammonium bromide (CTAB)* and was stirred for 20 h. Then, the precipitate (black color) was filtered and well dried.

## 2.3. Surface modification of the prepared nanomaterial

$Fe_3O_4$@$SiO_2$ (0.06 g) was spread out in 2.2 ml of dry toluene by ultrasonication for 25 min under $N_2$. Then, 0.06 ml of $CeO_2$/CTAB was joined and was refluxed under nitrogen for 20 h. After completion of the reaction, the resulting $Fe_3O_4$@$SiO_2$@$CeO_2$ magnetic nanoparticles (FSC) were isolated by filtration, washed with acetone, and dried at room temperature [19-20]. All materials were used directly without any further purification.

## 2.4. Particle size and zeta potential distributions

The size distribution and particle size of the FSC/drug were characterized by photon correlation spectroscopy (PCS) using a Zetasizer 2300 Malvern Instruments, UK. This solution (including FSC/drug) was diluted with filtered (0.32μm) with ultra-pure water and analyzed using Zetasizer. The surface charge was determined using an aqueous dip cell in an automatic mode by placing diluted samples (with ultra-purified water) in the capillary measurement cell, and the cell position was adjusted [23-25]. The particle size of HA/casein nanoparticles was measured using Dynamic Light Scattering (DLS) technique (ZS/ZEN3600 Zeta sizer; Malvern, Instruments Ltd, Malvern, UK).

## 2.5. Loading and release studies of Celecoxib

The Celecoxib loading was studied by adding FSC (0.005 g) into a phosphate buffer (5 ml, pH 3.3) containing celecoxib (0.07 mM in ethanol) with magnetic stirring at ٤٠ °C for ٤ h. Then, the mixture was isolated via an external magnet and was utilized for measuring the drug loading amount. To remove the unloaded celecoxib, the precipitate was re-dispersed in ٤ ml of the above buffer (Schematic 1). Uv-Vis quantified the free-celecoxib content at 253 nm. The amount of the loaded drug was calculated by Eq. (1) [26].

Loading content = $M_0$-$M_t$ /$M_N$ × 100 % Eq. (1)

Here, $M_0$ and $M_t$ are the amounts of celecoxib in the primary and filtered solutions, respectively. $M_N$ is the amount of FSC used for the loading process.

To determine the amount of the drug adsorbed after 120 min, 8, 24, and 48 h, 1 ml of the above solution was replaced with a fresh buffer solution and was analyzed by UV-Vis [27]. The loading process would be achieved via the hydrogen bonding interactions of the hydroxyl groups of celecoxib with the surface amino groups of FSC. To study the impact of drying conditions on the loading efficacy of the modified nanomaterial; the prepared final compound was dried under freeze conditions. Results showed only a little enhancement in the loading capacity compared with the one dried under usual thermal conditions.

This system was equipped with a 4 mV helium/neon laser at 633 nm wavelength and measured the particle size with the noninvasive backscattering technology at a detection angle of 173° after at least 100-fold dilution with purified water. The DLS measurements were performed at 25.0 ± 0.1 °C at 20-second intervals for three repeat measurements. Each diluted nanoparticle suspension was put in a universal folded capillary cell equipped with platinum electrodes for zeta potential measurement. The electrophoresis mobility was measured and the zeta potential (ζ) was calculated by the Dispersion Technology Software provided by Malvern.

Aliquots of 1 ml were withdrawn at pre-determined time intervals and immediately replaced by the same volume of the fresh medium. The aliquots were suitably diluted with the dissolution medium and analyzed by UV-Vis Spectrophotometer at the appropriate wavelength. Stability studies of prepared FSC nanoparticles were carried out by storing optimized formulation at 25 ± 1 °C and 40 ± 2 °C for 90 days. The samples were analyzed at 1-3 months for their drug content, drug release rate ($t_{50\%}$) as well as any changes in their physical appearance (ICH Q1A (*R*2) 2003) [28].

## 3. Results and discussion

Fig. 1a, b shows the FT-IR spectra of celecoxib, FSC, and celecoxib-loaded $Fe_3O_4$@$SiO_2$@$CeO_2$. The reaction of hydroxyl groups on the surface of $Fe_3O_4$@$SiO_2$ with the ethoxy groups of trimethoxysilylpropylamine ended in the formation of a novel carrier system. The bands at ٦48, 940, and 1069 $cm^{-1}$ are attributed to the Fe-O, Si-O-H, and, Si-O-Si vibrations, respectively. The bands at 648 $cm^{-1}$ in the FT-IR spectrum were ascribed to Ce–O stretching vibration, which corroborated that it is cross to the surface of nanomagnetic material. The grafted Ce–O groups at the surface of FSC formed H-bond with the oxygen atoms of celecoxib, causing the drug molecules to settle down onto the carrier surface Fig. 1a [29-30].

According to the chemical structure of celecoxib, the presence of S=O stretching vibration at 1339 $cm^{-1}$, together with aliphatic C–H stretching vibrations in 2925–2986 $cm^{-1}$ for the alkyl groups confirmed loading of the celecoxib. Moreover, the bands at 1090, 1437, and 1561 $cm^{-1}$ are assigned to C-N, C-H, and N-H bending vibrations, respectively Fig. 1b.

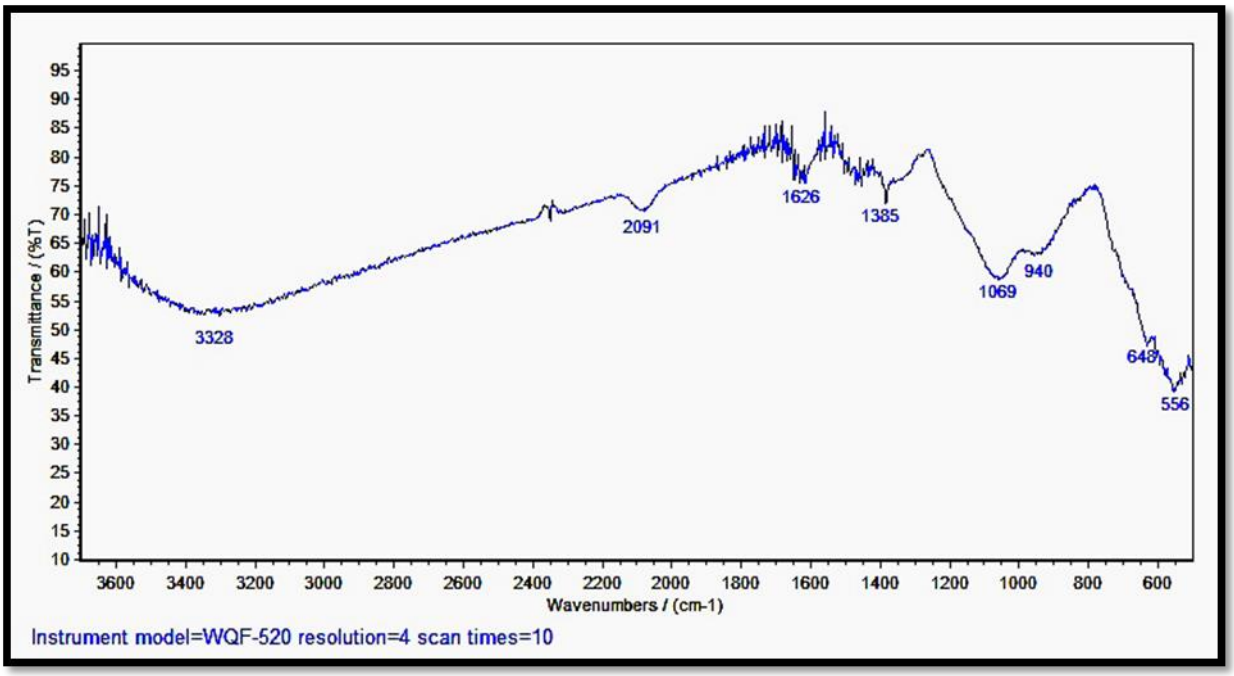


a)

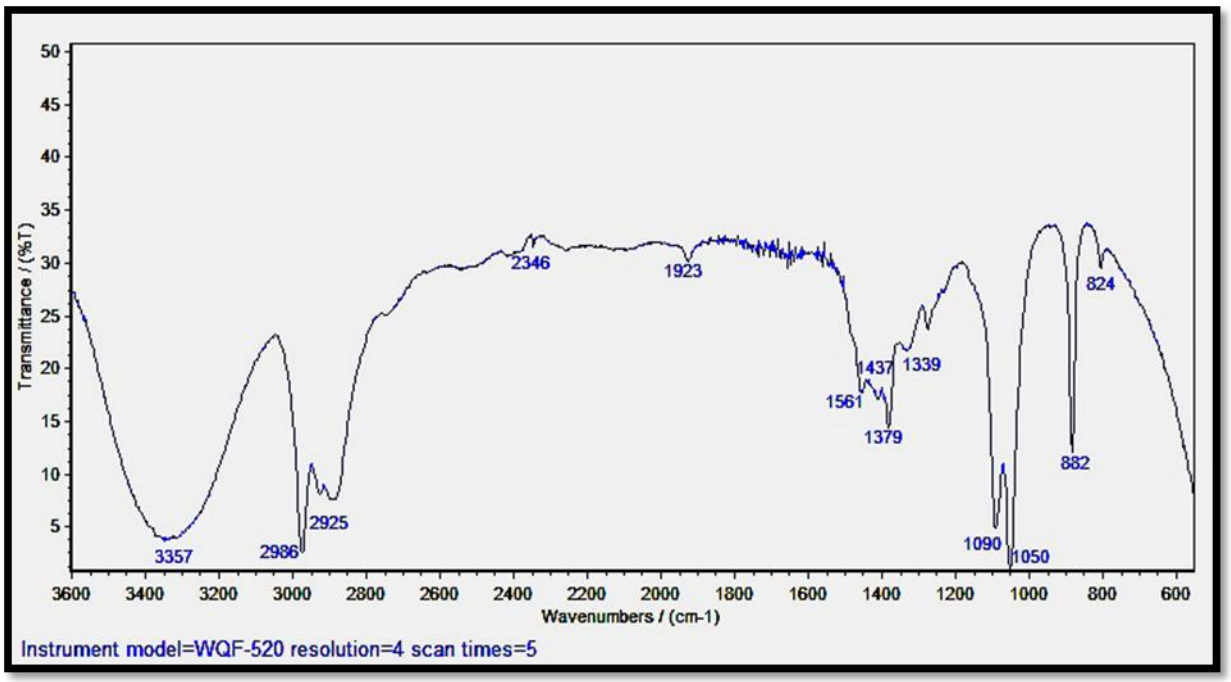


**b)**

**Fig. 1.** FT-IR spectra of FSC (a), and celecoxib loaded $Fe_3O_4$@$SiO_2$@$CeO_2$ (b).

The XRD patterns for $Fe_3O_4$ and drug-loaded $Fe_3O_4$@$SiO_2$@$CeO_2$ (FSC) are depicted in Fig. 2. It is assigned that the relative intensities and positions of the reflection peaks for $Fe_3O_4$ nanoparticles agree well with the standard diffraction card JCPDS 12882-54552. Comparing the XRD pattern of initial $Fe_3O_4$ nanoparticles to the modified one displayed that the pores remained intact after functionalization (Fig. 3) [31]. The attendance of a distinct peak at nearly $2\theta$ = 25-35°, which matches with the reported ones, authenticated that the pores retained after functionalization and the structure of magnetite remained intact after drug loading.

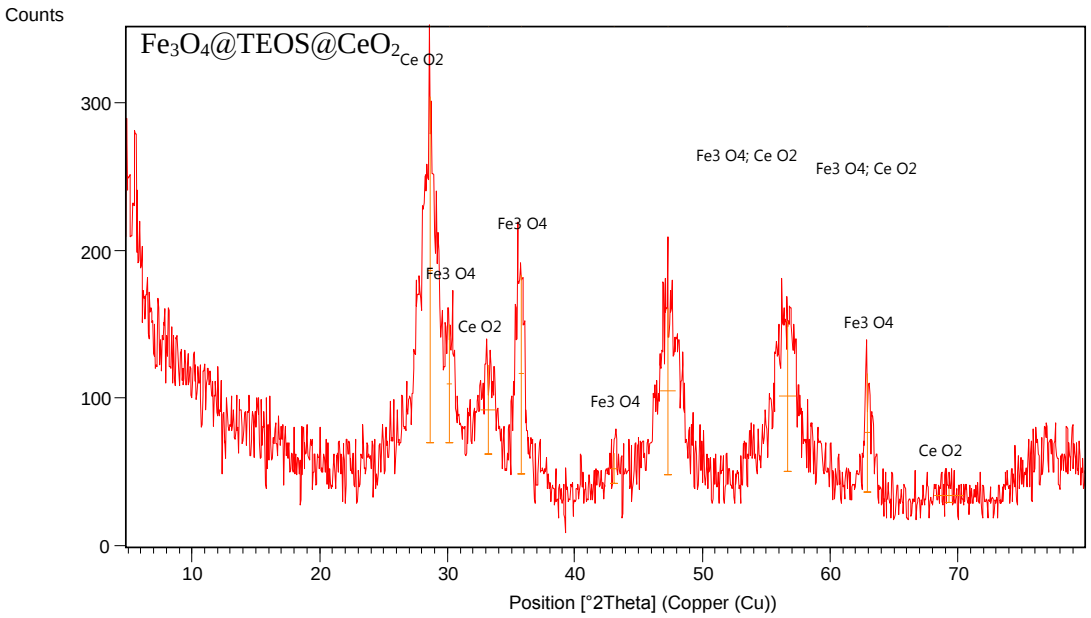


**Fig. 2.** XRD pattern of $Fe_3O_4@SiO_2@CeO_2$ (FSC) nanocomposite.

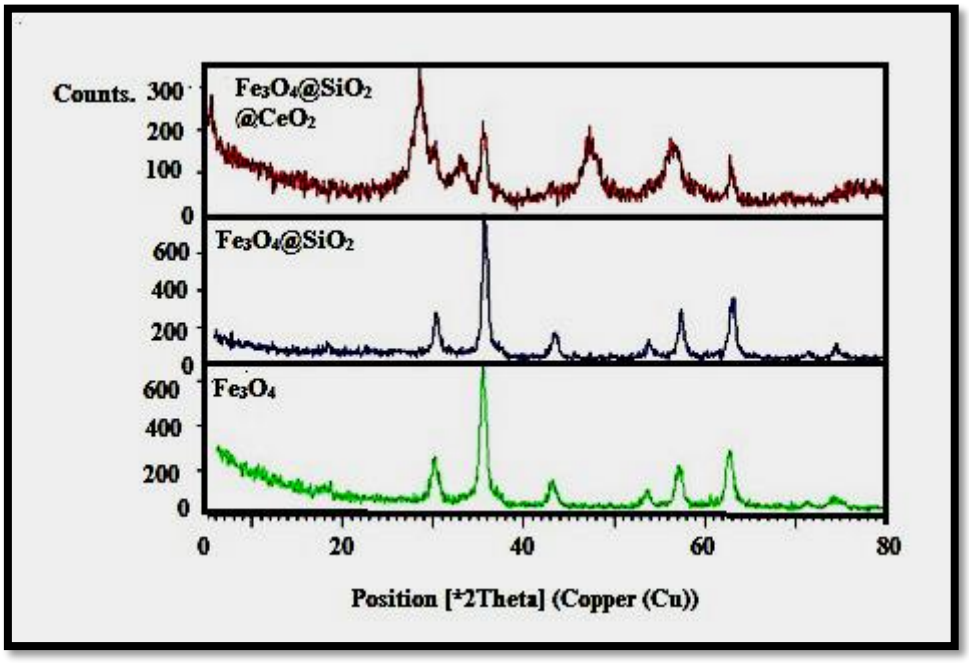


**Fig. 3.** Compare the resulting pattern XRD pattern of $Fe_3O_4$, $Fe_3O_4@SiO_2$ (FS), $Fe_3O_4@SiO_2@CeO_2$ (FSC) nanocomposite.

Zetasizer analyzed the particle size of Celecoxib/FSC nanoparticles loaded. EDX spectroscopic results related to the FSC nanocomposite coating containing cerium oxide and silica are reported in Fig. 4. The EDX spectrum of this nanocomposite shows the presence of Fe, Si, Ce, O, C elements. X-ray diffraction analysis and the presence of corresponding peaks confirm the presence of cerium and silica nanoparticles in this nanocomposite. The Z-particle size (r.nm) of Celecoxib/FSC nanoparticles formulations ranged from 2.9 to 13.3 nm, as shown in Table 1. Particle size and zeta potential result revealed that all nanoformulation were within the range of 2.9 to 13.3 nm, with the slight negative in charge.

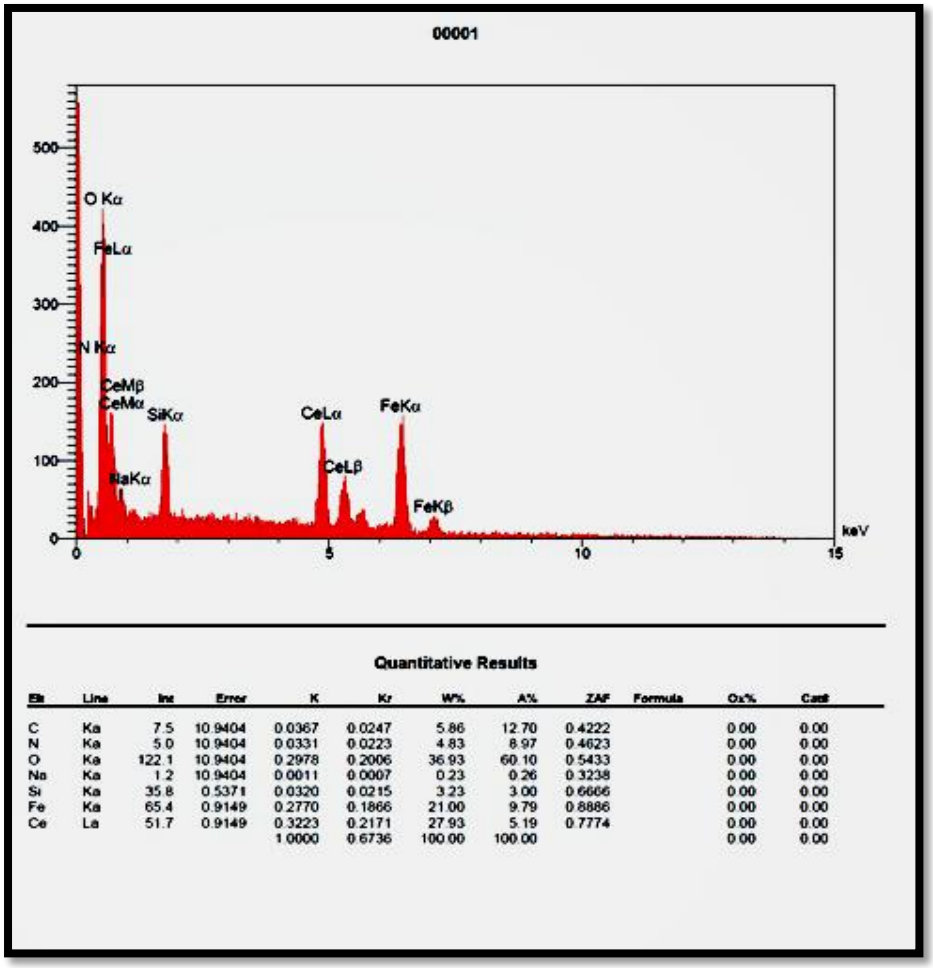


**Fig. 4.** Spectrum of EDX and size distribution of $Fe_3O_4$@$SiO_2$@$CeO_2$ (FSC) anocomposite.

**Table 1.** Evaluation of particle size and zeta potential.

| Formulation | Particle Size | | Zeta Potential (mV) |
|---|---|---|---|
| | Size (r.nm) | Mean Intensity (%) | |
| FSC | 2.903 | 41.8 | -5.17 |
| | 4.128 | 58.2 | |
| FSC | 11.157 | 31.7 | -6.18 |
| | 13.30 | 68.3 | |

In this respect, the dimensions (size and surface) characteristics of nanoparticles are of prime importance. Particles of 50 nm diameter with hydrophilic surfaces have a longer circulation in the blood and increase the targeting efficiencies to specific sites [28-29]. The electric charge present on the FSC nanoparticles was evaluated by measuring the zeta potential. The zeta potential of FSC nanoparticles was in the range of -6.18 to -5.17 mV (Table 1) which indicates no agglomeration, meanwhile with moderate stability.

Scanning electron microscopy micrograph of optimized Celecoxib/FSC nanoparticles showed that the particles have a smooth surface and they are uniformly and spherically distributed (Fig. 5). The size and morphology of $Fe_3O_4$ and FSC were further studied with FESEM. Fig. 5 describes that $Fe_3O_4$ nanoparticles were semi-spherical in shape; therefore, the prepared $Fe_3O_4$ nanoparticles by solvothermal method resulted in uniform sizes with good dispersibility. The images dispersion of transmission electron microscopic (TEM) of FSC nanoparticulate (Fig. 6) further confirms the spherical shape of nanoparticles with less or no aggregation. The average grain size obtained by XRD via the Scherrer equation for $Fe_3O_4$ (<30 nm) was in good agreement with the results obtained by FESEM (<25 nm). The FESEM images for FSC nanocomposites before and after drug loading confirmed that the semi-spherical shape of the nanoparticles was unchanged and no observable change in morphology of the nanoparticles occurred.

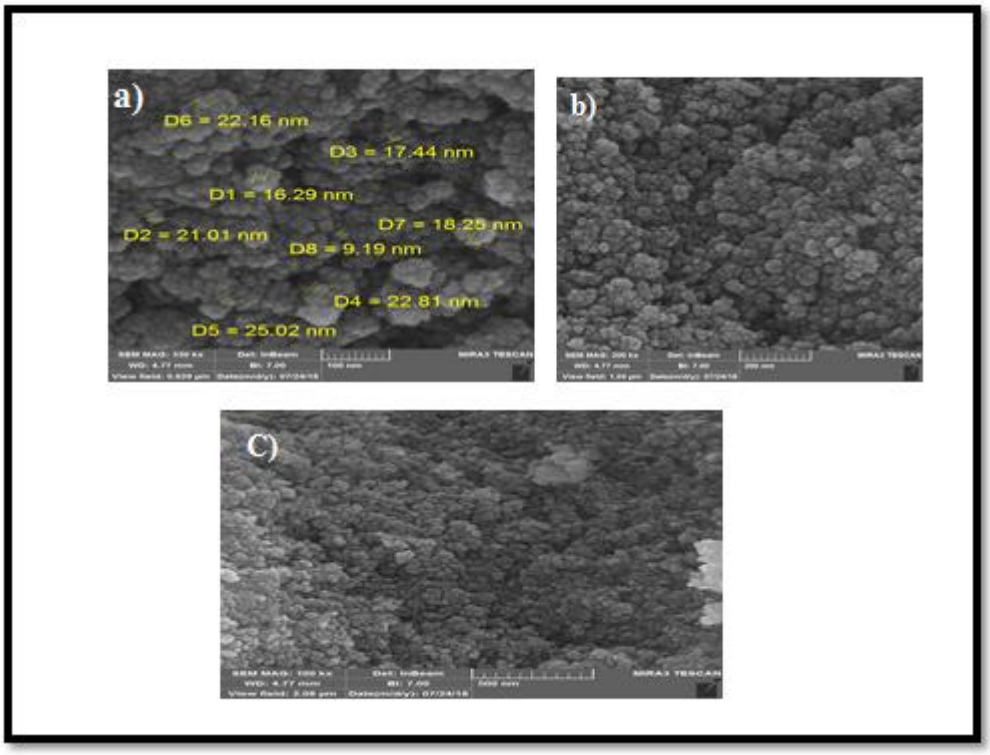


**Fig. 5.** FESEM images of the FSC with resolution of (a) 100 nm, (b) 200 nm, (c) 500 nm.

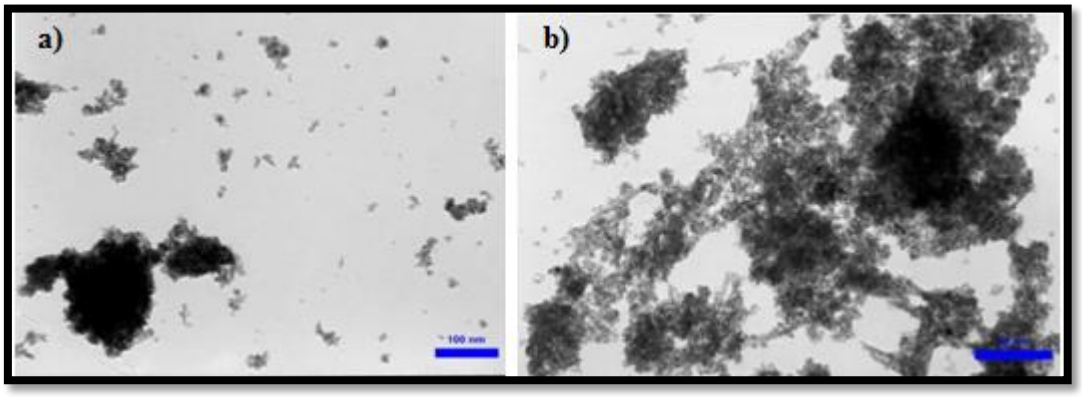


**Fig. 6**. (a, b). TEM images of the $Fe_3O_4$@$SiO_2$@$CeO_2$ (FSC).

Considering the d-orbital of Ce and the influence of hydrogen bonding on the loading of the drug onto the pores of the modified nanomagnetic material, further studies were outlined to clarify loading and release efficacies. The pH, loading time, and temperature seem to be the main parameters on the celecoxib loading.

The impact of pH on celecoxib loading was investigated using a variety of pHs ranging from acidic to basic. As Fig. 7 shows, for the increments of the hydrogenic interactions in an alkaline pH, the best loading can be achieved at pH 3.3. The decrease in loading was observed at high alkaline pH (>7) merely due to the hydrolysis of Fe–O–Si and C-O-Si bands and demolition of the bind to the agent. The loading temperature was also screened on the drug loading capacity. Findings displayed that by enhancing temperature, the drug loading improves. This phenomenon can be attributed to decreasing desorption because of the hydrogenic interactions by raising temperature [32]. The effect of time on the loading of celecoxib onto FSC was also investigated.

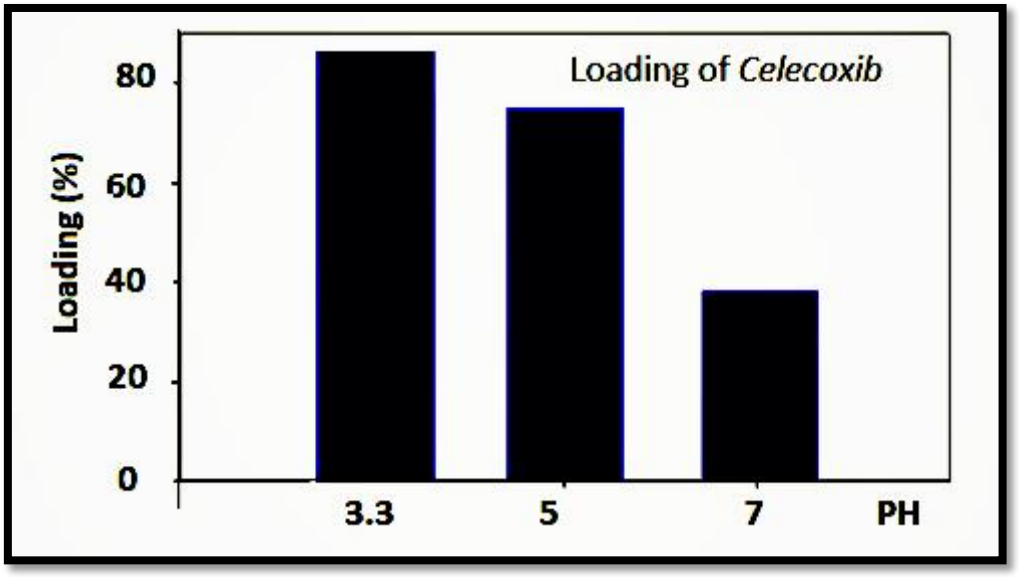


**Fig. 7**. Effect of pH on loading of celecoxib onto FSC.

Dynamic light scattering (DLS) is a valuable tool for studying size and degree of agglomeration of the nanoparticles as a function of time in the suspension solution. In this technique, one can determine the hydrodynamic size of the nanoparticles by measuring the intensity of laser scattered light that passes through a colloidal solution. Larger particles will diffuse slower than smaller particles. So, particle size can be mathematically provided by measuring the time dependence of the scattered light. The DLS experimental data obtained in this work which is given in Fig.8, shows a zeta particle size distribution of 45 nm. In fact, this is the average particle size of the FSC nanocomposite prepared on $Fe_3O_4@SiO_2$ (FS). The zeta-potential (Fig. 9)of the particles, which is a basic parameter in controlling the stability of colloidal suspensions, is obtained by measuring particles mobility under an applied electric field which is applied and can be calculated using the Smoluchowski equation [33]:

$$\zeta = \frac{\eta}{\varepsilon_0.\varepsilon_r} U \qquad (2)$$

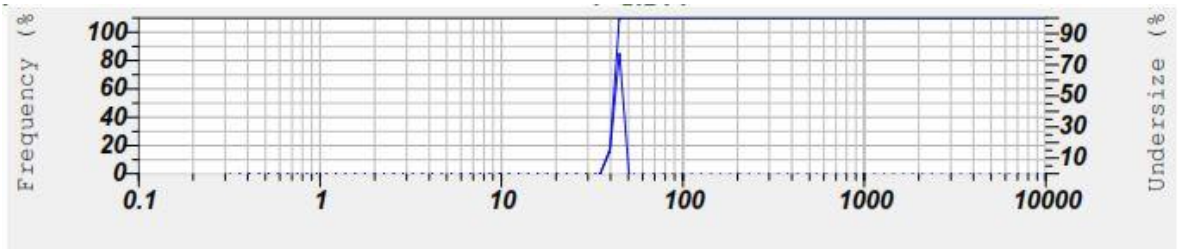


**Fig. 8.** DLS measured results for FSC nanocomposite prepared on $Fe_3O_4@SiO_2$ (FS).

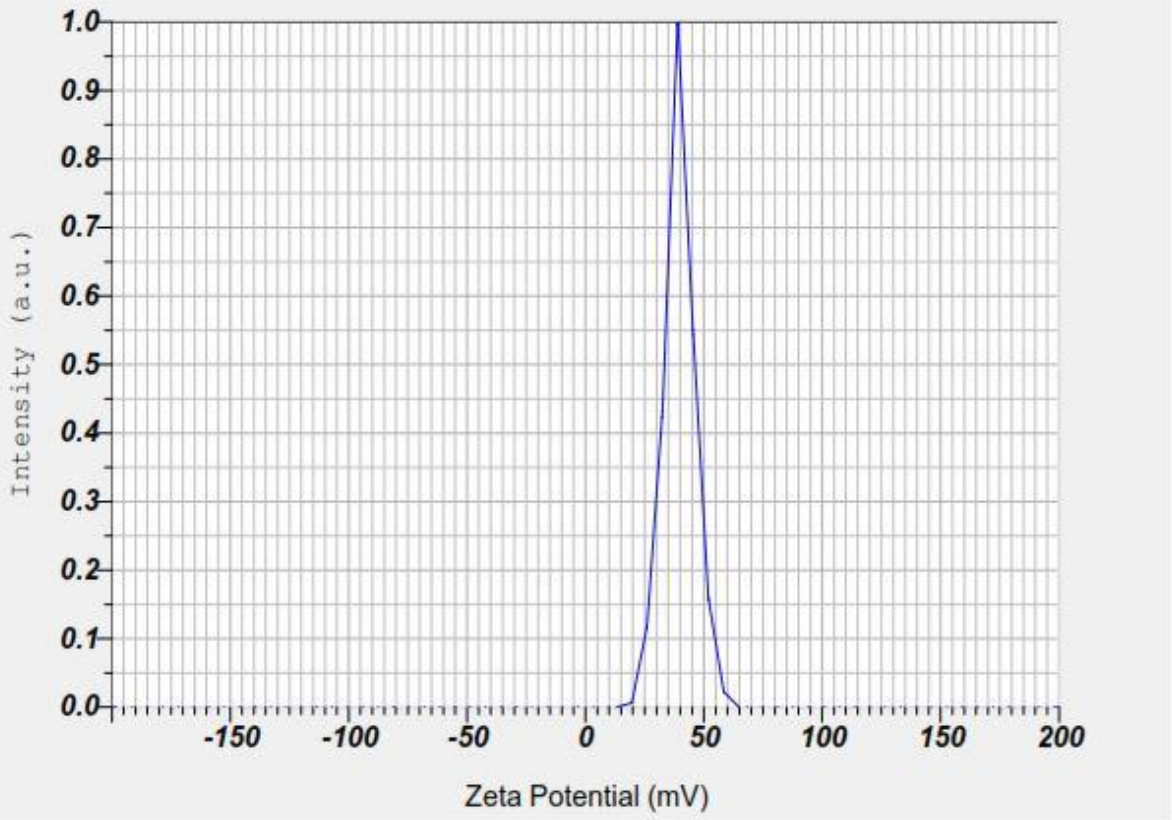


**Fig. 9.** Zeta potential distributions for FSC nanocomposite prepared on $Fe_3O_4$@$SiO_2$ (FS).

Where, $\varepsilon_0$ and $\varepsilon r$ are dielectric constants of vacuum and solvent respectively, $\eta$ is viscosity and U is the mobility of the particles in suspended solution. In general, when an electric field is applied to the charged particles in a colloidal sample, particles move toward an electrode opposite to its surface charge. Because the velocity is proportional to the amount of charge of the particles, zeta potential can be therefore estimated by measuring the mobility of these particles. To determine the speed of the particles movement, the particles was normally irradiated with laser light, and the light emitted from the particles was detected from the shifted scattered frequency. Since shifted scattered light from incident light is proportional to the speed of the movement of the particles, the electrophoretic mobility of the particles can be thereby measured [34-37]. The most widely used theory for calculating zeta potential from experimental data was developed by Marian Smoluchowski in 1903 [37].

Experimental zeta potential value obtained in this work for FSC nanocomposite prepared on $Fe_3O_4$@$SiO_2$ (FS) is given in Fig. 9. This result reveals a bimodal zeta potential distribution may be due to the two different populations of particles within the prepared suspension sample. About 42% of the particles have a zeta potential of +50 mV, and 58% of the particles have a lower value of +40.94 mV. Considering that and a dividing line between stable and unstable aqueous dispersions reported at either +15 or +65mV, particles with zeta potentials more positive than +30mV have been considered stable, and particles with low absolute values of the zeta potential will agglomerate, and the dispersion becomes unstable [38-46], we can conclude that colloidal samples prepared in this work at the our experimental condition even after 4 hours ultrasonic treatment, were unstable because of FSC nanocomposite high tendency to aggregate.

Considering the important role of temperature on the drug loading and the body temperature, three different temperatures 35, 43, and 50 °C were investigated (Fig. 10). Results showed that by increasing temperature, the drug loading was increased, and the best loading was achieved at 50 °C.

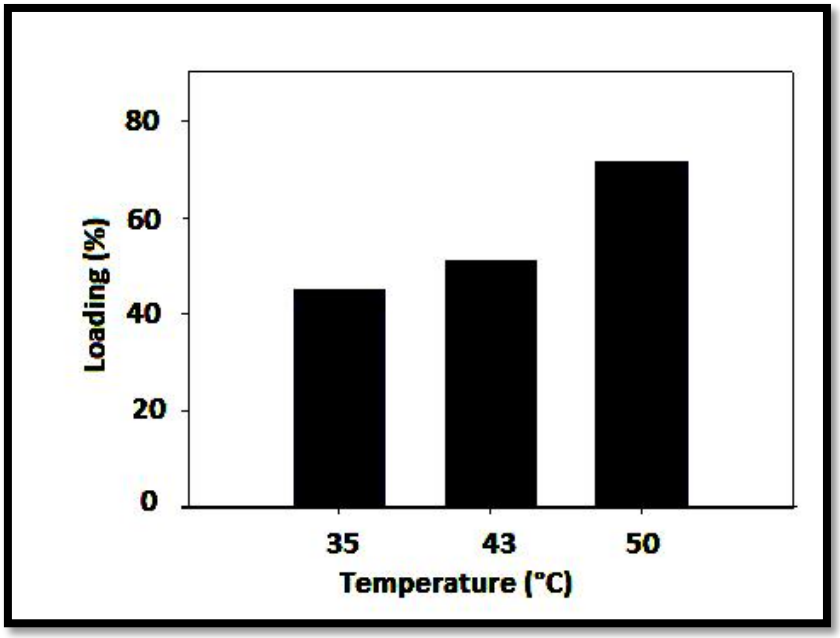


**Fig. 10.** Effect of temperature on loading of celecoxib onto FSC.

According to the diagram with equation Y=19.883X+0.0025, the correlation coefficient for equation 0.999 has been calculated, which is desirable (Table 2, Fig. 11). According to the results, the only mechanism of drug release from nanocomposite in solution was the Fickian model, and matrix degradation did not have the main role in the release of *Celecoxib*. The early high-level release is probably due to the release of *Celecoxib* on the surface of the nanocomposite that was matched with the Higuchi model (Table 3). Therefore, because of the heavy-metal degradation of the FSC, the release mechanism does not match with the Hixon-Crowell model. The greatest value of the correlation coefficient ($r^2$) was obtained from the Higuchi model. In addition, the correlation coefficient for the different release rates of the drug from FSC explains relative adaptation to the First-order model. This model is related to the delivery of poorly soluble drugs into the release medium. In addition to Fickian theory, four more models were used to analyze the drug-release profile further, including the first order, Higuchi, and Hixon–Crowell models. These model equations are listed as follows:

First order: $\ln Q_t = \ln Q_0 + K_1 t$ (3)

Hixson–Crowell: $Q_0^{1/3} - Q_t^{1/3} = K_s t$ (4)

Higuchi: $Q_t = K_H \sqrt{t}$ (5)

$Q_t$ is the amount of drug dissolved in time t, $Q_0$ is the initial amount of drug in the solution (most of the time, $Q_0^{1/4}$), $K_1$ is the first-order release constant, $K_H$ is the Higuchi dissolution constant, and $K_S$ is a constant incorporating the surface–volume relation [31-32].

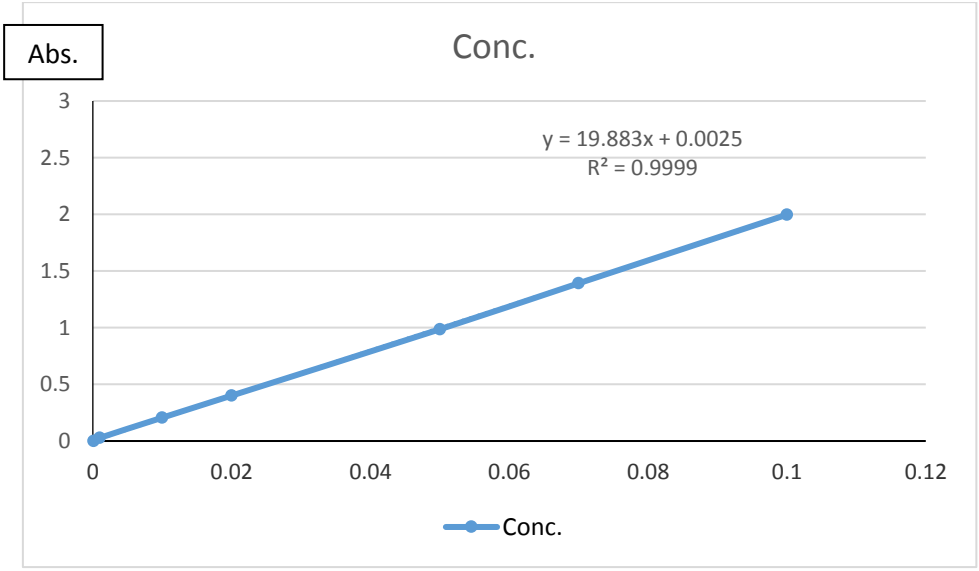


**Fig. 11.** Celecoxib calibration curve onto FSC.

**Table 2.** Results of celecoxib adsorption.

| Conc. (mM) | Absorbsion |
|---|---|
| 0.0001 | 0 |
| 0. 001 | 0.028 |
| 0.01 | 0.206 |
| 0.02 | 0.401 |
| 0.05 | 0.986 |
| 0.07 | 1.392 |
| 0.1 | 1.997 |

**Table 3**. Regression coefficients of mathematical models fitted to the release of *Celecoxib* from the FSC- *Celecoxib* nanocomposites mats.

| samples | Zero order | First order | Hixson–Crowell | Higuchi |
|---|---|---|---|---|
| FSC- *Celecoxib* | 0.37 ± 0.03 | 0.61 ± 0.06 | 0.4 ± 0.01 | 0.8 ± 0.09 |

Stability studies of Celecoxib/FSC were carried out by storing optimized formulation at 4 ± 1 °C and 30 ± 2 °C for 3 months. The samples were analyzed at 1-3 months for their drug content and drug release rate ($t_{50\%}$), as well as any changes in their physical appearance (Table 4). These results indicated that the developed Celecoxib/FSC nanoparticles retain their pharmaceutical properties at various environmental conditions over a period of 3 months and are physically/chemically stable.

Thermogravimetric analysis (TGA) traces of $Fe_3O_4$@$SiO_2$@$CeO_2$ magnetic nanoparticles are illustrated in Fig. 12. TGA of $Fe_3O_4$ exhibits 9% weight loss because of the removal of water molecules and surface hydroxyl groups (Fe−OH) [44], whereas that of $Fe_3O_4$@$SiO_2$@$CeO_2$ contains two weight losses in the range 180−210 and 500−680 °C. The first weight loss is attributed to the dehydration of $CeO_2$. Similar TGA behavior was observed by Yang and co-workers in nanoceria prepared by the solvothermal synthesis in ethylene glycol [48]. TGA analysis revealed that, apart from the solvent mass loss, all samples underwent large weight loss in the temperature range 205–395 °C (13–26%) accompanied by endothermic processes [46], probably due to oxalate decomposition and leaching of organic ligands [49], that formed an inorganic–organic composite with ceria.

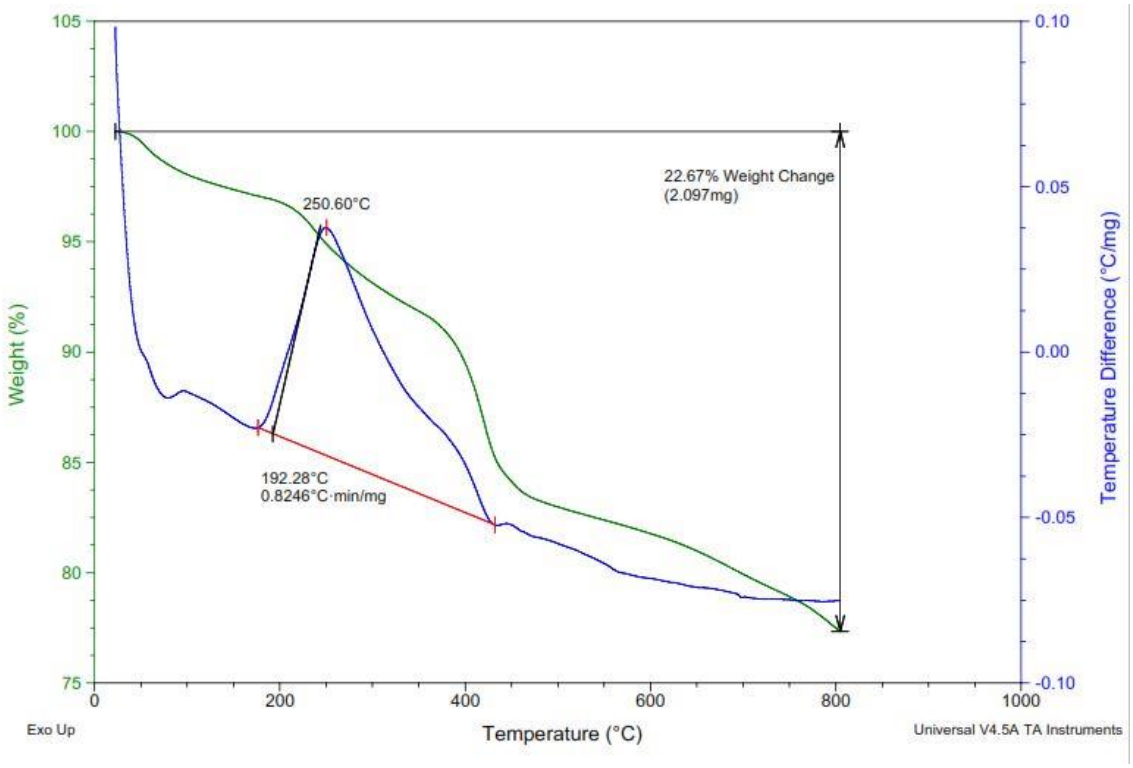


**Fig. 12.** TGA curves of $Fe_3O_4$@$SiO_2$@$CeO_2$ (FSC) in the range 0−1000°C.

**Table 4**. Regression coefficients of mathematical models fitted to the release of *Celecoxib* from the FSC- *Celecoxib* nanocomposites.

| Temperature | Evaluation Parameters | Observation (Months) | | | |
|---|---|---|---|---|---|
| | | 0 | 1 | 2 | 3 |
| 40°C ± 2°C | Physical appearance | --- | No change | No change | No change |
| | %Drug content | 77.15 | 74.65 | 73.45 | 71.86 |
| | $t_{50\%}$ (hrs) | 13.85 | 13.18 | 12.90 | 12.75 |
| 8°C ±1°C | Physical appearance | --- | No change | No change | No change |
| | %Drug content | 77.15 | 75.67 | 74.91 | 72.88 |
| | $t_{50\%}$ (hrs) | 13.85 | 13.65 | 13.16 | 12.92 |

## 4. Conclusions

In this study, celecoxib/FSC nanoparticles were successfully prepared by the modified nanoprecipitation method. Magnetite $Fe_3O_4$@$SiO_2$ nanoparticles are synthesized by the sol-gel method. In summary, the uniform $Fe_3O_4$ nanoparticles were successfully synthesized, and then the prepared nanoparticles were enriched with silanol groups and were finally modified with TMPA to improve their efficiencies in the delivery of celecoxib. The introduced biocompatible delivery system showed a very good capacity for the storage of a large amount of celecoxib. The two important parameters of pH and amounts of the nanocomposite were investigated. In order to show the necessity of modification, the efficiency of the FSC nanomaterial was compared with FSC, and the results demonstrated that modification has been absolutely effective. With respect to particle size entrapment efficiency, it can be included that the formulation ($m_{FSC}$=5 mg, pH=3.3) was considered to be the best among various formulations. The pH and concentration of biomaterial used for formulating these batches of nanoparticles showed a significant effect on its efficiency to entrap the Celecoxib molecule. Dynamic light scattering (DLS) techniques used to measure particle size and zeta potential distribution revealed successful preparation of the FSC nanocomposite prepared on $Fe_3O_4$@$SiO_2$ (FS), with a hydrodynamic size distribution of 45 nm. Bimodal zeta potential distribution in divergence with the DLS average zeta size data reveals the instability of the FSC nanocomposite because of casein- calcium nanocomposite's high tendency to aggregation. Cerium oxide displaces electron transfer and absorption band due to the presence of f-orbital in the cerium network.

**ETHICS APPROVAL AND CONSENT TO PARTICIPATE**

Not applicable.

**HUMAN AND ANIMAL RIGHTS**

No animals/humans were used for the studies that are the basis of this research.

**CONSENT FOR PUBLICATION**

Not applicable.

**AVAILABILITY OF DATA AND MATERIALS**

Not applicable.

## ACKNOWLEDGMENTS

The financial support and encouragement support was provided by the Research vice Presidency of North Tehran Branch, Islamic Azad University and Executive Director of Iran-Nanotechnology Organization (Govt. of Iran), and Executive Director of Iran-Nanotechnology Organization (Govt. of Iran).

**References**

[1] Van, R. S.; Habibovic, P. Enhancing regenerative approaches with nanoparticles. J. R. Soc. Interf. Vol. 14, No. 129, 2017, pp. 20170093.

[2] Conte, R.; Marturano, V.; Peluso, G. Recent advances in nanoparticle-mediated delivery of anti-inflammatory phytocompounds. Int. J. Mol. Sci. Vol. 18, No. 4, 2017, pp. 709-714.

[3] Arbos, P.; Campanero, M. A.; Arangoa, M. A.; Renedo, M. J.; Irache, J. M. Influence of the surface characteristics of PVM/ MA nanoparticles on their bioadhesive properties. J. Control. Release. Vol. 89, No. 1, 2003, pp. 19-30.

[4] Ginebra, M. P.; Traykova, T.; Planell, J. A. Calcium phosphate cements as bone drug delivery systems: A review. J. Control. Rel. Vol. 113, No. 2, 2006, pp. 102-107.

[5] Patri, A. K.; Majoros, L. J.; Baker, J. R. Dendritic polymer macromolecular carriers for drug delivery. Curr. Opin. Chem. Bio. Vol. 6, No. 4, 2002, pp. 466-471.

[6] Rezwan, K.; Chen, Q. Z.; Blaker, J. J.; Boccaccini, A. R. Biodegradable and bioactive porous polymer/inorganic composite scaffolds for bone tissue engineering. Biomater. Vol. 27, No. 18, 2006, pp. 3413-3431.
[7] Horcajada, P.; Chalati, T.; Serre, C.; Gillet, B.; Sebrie, C. Porous metal-organic-framework nanoscale carriers as a potential platform for drug delivery and imaging. Nat. Mater. Vol. 9, 2010, pp. 172-178.
[8] Zahir Abadi, I. J.; Sadeghi, O.; Lotfizadeh, H. R.; Tavassoli, N.; Amani, V.; Amini, M. M. Novel modified manoporous silica for oral drug delivery: Loading and release of clarithromycin. J. Sol Gel Sci. Technol. Vol. 61, No. 1, 2012, pp. 90-95.
[9] Tang, F.; Li, L.; Chen, D. Mesoporous silica nanoparticles: Synthesis, biocompatibility and drug delivery. Adv. Mater. Vol. 24, No. 12, 2012, pp. 1504-1534.
[10] Van, R. S.; Habibovic, P. Enhancing regenerative approaches with nanoparticlesJ. R. Soc. Interf. Vol. 14, No. 129, 2017, pp. 20170093.
[11] Tang, Q.; Xu, Y.; Wu, D.; Sun, Y.; Wang, J. Studies on a new carrier of trimethylsilyl-modified mesoporous material for controlled drug delivery. Control. Rel. Vol. 114, No. 1, 2006, pp. 41-46.
[12] Trewyn, B. G.; Giri, S.; Slowing, I. I.; Lin, V. S. Y. Mesoporous silica nanoparticle based controlled release, drug delivery and biosensor systems. Chem. Commun. Vol. 31, No. 3, 2007, pp. 3236-3241.
[13] Yang, Q.; Wang, S. H.; Fan, P.; Wang, L.; Di, Y.; Lin, K.; Xiao, F. S. pH-responsive carrier system based on carboxylic acid modified mesoporous silica and polyelectrolyte for drug delivery. Chem. Mater. Vol. 17, No. 1, 2005, pp. 59-68.
[14] Chomchoey, N.; Bhongsuwan, D.; Bhongsuwan, T. Magnetic properties of magnetite nanoparticles synthesized by oxidative alkaline hydrolysis of iron powder. J. Nat. Sci. Vol. 44, No. 12, 2010, pp. 963-971.
[15] Hoa, L. T. M.; Dung, T. T.; Danh, T. M.; Duc, N. H.; Chien, D. M. Preparation and characterization of magnetic nanoparticles coated with polyethylene glycol. J. Phys. Vol. 187, No. 1, 2009, pp. 12-18.
[16] Acar, H. Y. C.; Garaas, R. S.; Syud, F.; Bonitatebus, P.; Kulkarni, A. M. Superparamagnetic nanoparticles stabilized by polymerized PEGylated coatings. J. Magn. Magn. Mater. Vol. 293, No. 1, 2005, pp. 1-7.
[17] Mohammadyan, E.; Ghafuri, H.; Kakanejadifard, A.; Synthesis and characterization of a magnetic $Fe_3O_4$@$CeO_2$ nanocomposite decorated with Ag nanoparticle and investigation of synergistic effects of Ag on photocatalytic activity. Optik. Vol. 166, 2018, pp. 39-48.
[18] Moradi, B.; Nabiyouni, Gh. R,; Ghanbari, D.; Rapid photo-degradation of toxic dye pollutants: green synthesis of mono-disperse $Fe_3O_4$–$CeO_2$ nanocomposites in the presence of lemon extract. J. Mater. Sci: Mater. Elect. Vol. 29, No. 5-6, 2018, pp.11065-11080.
[19] Rizzuti, A.; Dipalo, C. M.; Allegereta, I.; Terzano, R.; Cioffi, N.; Microwave-assisted solvothermal synthesis of $Fe_3O_4$–$CeO_2$ nanocomposite and their catalytic activity in the imine formation from benzyl alcohol and aniline. Catalyst. Vol. 10, No. 1325, 2020, pp. 1-22.
[20] Channei, D.; Inceesungvorn, B.; Wetchakun, N.; Phanichphant, S. Synthesis of $Fe_3O_4$/$SiO_2$/$CeO_2$ core-shell magnetic and their application as photocatalyst. J. Nanosci. Nanotechnol. Vol. 14, No. 10, 2014, pp. 7756-7762.
[21] Huang, Y.; Zhang, L.; Huan, W.; Xiaojuan, L.; Yang, Y. A study on synthesis and properties of $Fe_3O_4$ nanoparticles by solvothermal method. Glass Phys. Chem. Vol. 36, No. 3, 2010, pp. 325-331.
[22] Saadatjooa, N.; Golshekana, M. Organic/inorganic MCM-41 magnetite nanocomposite as a solid acid catalyst for synthesis of benzo [α] xanthenone derivatives. J. Mol. Cat. A: Chem. Vol. 377, No. 5, 2013, pp. 173-179.
[23] Donga, Y.; Wai, K. N.; Shen, S.; Kim, S.; Tan, R. B. H. Preparation and characterization of spironolactone nanoparticles by antisolvent precipitation. Int. J. Pharm. Vol. 375, No. 1-2, 2009, pp. 84-88.
[24] Maniya, N. H.; Sanjaykumar, R. P.; Murthy, Z. V. P. Controlled delivery of celecoxib from porous silicon micro- and nanoparticles. Appl. Sur. Sci. Vol. 330, No. 8, 2015, pp. 358-363.
[25] Huang, S. T.; Du, Y. Z. Synthesis and anti-hepatitis B virus activity of celecoxib conjugated stearic acid-g-chitosan oligosaccharide micelle. Carbohydr. Polym. Vol. 83, No. 18, 2001, pp. 1715-1722.
[26] Dandagi, P.; Patel, P.; Mastiholimath, V.; Gadad, A. Development and characterization of a particulate drug delivery systemfor etoposide. Ind. J. Novel Drug Deliv. Vol. 3, No. 1, 2001, pp. 43-51.
[27] Liu, X.; Ma, Z.; Xing, J.; Liu, H. Preparation and characterization of amino–silane modified superparamagnetic silica nanospheres. J. Magn. Magn. Mater. Vol. 270, No. 1-2, 2004, pp. 1-6.
[28] Masteri-Farahani, M.; Tayyebi, N. A new magnetically recoverable nanocatalyst for epoxidation of olefins. J. Mol. Catal. A: Chem. Vol. 348, No. 1, 2011, pp. 83-88.
[29] Banerjee, S. S.; Chen, D. H. Magnetic nanoparticles grafted with cyclodextrin for hydrophobic drug delivery. Chem. Mater. Vol. 19, No. 25, 2007, pp. 6345-6349.

[30] Allemann, E.; Gurny, R.; Deolker, E. Drug loaded nanoparticles: preparation methods and drug targeting issues. Eur. J. Pharm. Biopharm. Vol. 39, No. 5, 1993, pp. 173-191.
[31] Banerjee, T.; Mitra, S.; Singh, A. K.; Sharma, R. K.; Maitra, A. Preparation and biodistribution of ultrafine chitosan nanoparticles. Int. J. Pharm. Vol. 243, No. 1-2, 2002, pp. 93-105.
[32] Moazzen, E.; Ebrahimzadeh, H.; Amini, M.; Sadeghi, O. J. A novel biocompatible drug carrier for oral delivery and controlled release of antibiotic drug: Loading and release of clarithromycin as an antibiotic drug model. Sol Gel Sci. Technol. Vol. 66, No. 5, 2013, pp. 345-352.
[33] Rodríguez-Lugo V., Salinas-Rodríguez E., Vázquez R. A., Alemán K., Rivera A. L., Hydroxyapatite synthesis from a starfish and β-tricalcium phosphate using a hydrothermal method. RSC Adv. Vol. 7, No. 13, 2017, pp. 7631-7639.
[34] Shahmohammadi M., Jahandideh R., Behnamghader A., Rangie M., Sol-gel synthesis of FHA/CDHA nanoparticles with a nonstochiometric ratio. Int. J. Nano Dimens. Vol. 1, No. 1, 2010, pp. 41-45.
[35] Wang J. P., Chen Y. Z., Yuan S. J., Sheng G. P., Yu H. Q., Synthesis and characterization of a novel cationic chitosan-based flocculant with a high water-solubility for pulp mill wastewater treatment. Vol. 43, No. 20, (2009), pp. 5267-5275.
[36] De Bruyn J. R., Goiko M., Mozaffari M., Bator D., Dauphinee R. L., Dynamic light scattering study of inhibition of nucleation and growth of hydroxyapitate crystals by osteopontin. Plus One. Vol. 8, No. 55, (2013), pp. 56764-56768.
[37] Lyklema J., Fundamentals of interface and colloid science. Vol. 2, (1995), pp. 3-208. ISBN 0-12-460529-X.
[38] Russel W. B., Saville D. A., Schowalter W. R., Colloidal dispersions, cambridge university press. (1992), ISBN 0-521-42600-6.
[39] Dukhin A. S., Goetz P. J., Ultrasound for characterizing colloids. Elsevier. (2002), ISBN 0-444-51164-4.
[40] Hunter R. J., Foundations of colloid science, Oxford University Press. (1989), ISBN 0-19-855189-4.
[41] Smoluchowski M., Contribution to the theory of electro-osmosis and related phenomena. Bull. Int. Acad. Sci. Cracovie. Vol. 3, No. 3, (1903), pp. 184-199.
[42] Morrison I. D., Ross S., Colloidal dispersions: Suspensions, emulsions, and Foams. (2002), ISBN 978-0-471-82848-8.
[43] Wang L., Li S., Phosphorylated osteopontin peptides inhibit crystallization by resisting the aggregation of calcium phosphate nanoparticles. Cryst. Eng. Comm. Vol. 14, No. 22, (2012), pp. 8037-8043.
[44] Sadjadi M. S., Meskinfam, M., Sadeghi B., Jazdarreh H., Zare K., In situ biomimetic synthesis, characterization and in vitro investigation of bone-like nanohydroxyapatite in starch matrix. Mat. Chem. Phys. Vol. 124, No. 1, (2010), pp. 217-222.
[45] Sadjadi M. S., Meskinfam, M., Sadeghi B., Jazdarreh H., Zare K., In situ biomimetic synthesis and characterization of nano hydroxyapatite in gelatin matrix. J. Biomedical Nanotech. Vol. 7, No. 3, (2011), pp. 450-454.
[46] Sadeghi B., Ghammamy Sh., Gholipour Z., Amini Nia A., Gold/hydroxypropyl cellulose hybrid nanocomposite constructed with more complete coverage of gold nano-shell. Mic. & Nano Lett. IET. Vol. 6, No. 4, (2011), pp. 209-213.
[47] Wu Y., Xing v, Zhou T., Zhao C., Examining the use of $Fe_3O_4$ nanoparticles to enhance the NH3 sensitivity of polypyrrole films. Poly. Bull. Vol. 59, No. 3, 2011, pp. 227-234.
[48] Zhang, J.; Yang, J.; Wang, J.; Ding, H.; Liu, Q.; Schubert, U.; Rui, Y.; Xu, J. Top of Form Bottom of Form Surface oxygen vacancies dominated $CeO_2$ as efficient catalyst for imine synthesis: Influences of different cerium precursors. J. Mol. Catal. Vol. 443, No. 2, 2017, pp. 131-138.
[49] De Almeida, L.; Grandjean, S.; Vigier, N.; Patisson, F. Insights into the thermal decomposition of Lanthanide(III) and Actinide(III) Oxalates – from neodymium and cerium to plutonium. Eur. J. Inorg. Chem. Vol. 31, No. 62, 2012, pp. 4986-4999.